International Journal of Pharmaceutics 665 (2024) 124676

Contents lists available at ScienceDirect

International Journal of Pharmaceutics

journal homepage: www.elsevier.com/locate/ijpharm

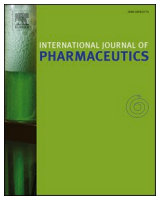

Hot Melt Extruded High-Dose Amorphous Solid Dispersions Containing Lumefantrine and Soluplus

Shu Li [a], Zi'an Zhang [a], Wenjie Gu [a], Maël Gallas [b,c], David Jones [a], Pascal Boulet [b], Lindsay M. Johnson [d], Victoire de Margerie [c], Gavin P Andrews [a,*]

[a] School of Pharmacy, Queen's University Belfast, 97 Lisburn Rd, Belfast BT9 7BL, NI UK
[b] Institut Jean Lamour, 2 allée André Guinier 54011 Nancy, France
[c] Rondol Industrie, 2 allée André Guinier 54011 Nancy, France
[d] BASF Corporation, 100 Park Avenue, Florham Park, NJ 07932, USA

ARTICLE INFO

Keywords:
Hot melt extrusion
High dose
Amorphous solid dispersions
Drug enablement
Lumefantrine
Soluplus
Anti-malarial

ABSTRACT

Over the last 15 years, a small number of paediatric artemisinin-based combination therapy products have been marketed. These included Riamet® and Coartem® dispersible tablets, a combination of artemether and lumefantrine, co-developed by the Medicines for Malaria Venture and Novartis. Disappointingly, patient compliance, requirement for high-fat meal, and sporadic drug dissolution behaviours following administration still result in considerable challenges for these products. The first and foremost barrier that needs addressed for successful delivery of the artemether/lumefantrine combination is the poor solubility of lumefantrine within the gastrointestinal fluids. In this work, amorphous solid dispersions of lumefantrine within Soluplus®-based matrices have been manufactured using hot melt extrusion as a potential formulation strategy to achieve enhanced dissolution and apparent solubility. The drug loading capacity of Soluplus® to accommodate amorphous lumefantrine, whilst ensuring improved in-vitro dissolution performance, was investigated. The extrusion process employed a variety of processing parameters, including various temperature profiles and different production scales. The influence of variation in extrusion conditions upon the physical stability of manufactured amorphous solid dispersions was also examined. This allowed for a greater understanding of the role of extrusion processing conditions on the performance of supersaturated amorphous solid dispersions during dissolution and storage. This may allow for the design and manufacture of drug enabled formulations with lower drug dosing and thus a lower risk of adverse effects.

1. Introduction

Malaria continues to be a life-threatening infectious disease with deaths occurring as fast as 24 h after initial onset of symptoms. In 2021, the global tally of malaria cases was reported to be 247 million, which resulted in 619,000 deaths (World Health Organization, 2022). Moreover, the same report also acknowledged that "children aged under 5 years, pregnant women, and people with HIV or AIDS are at higher risk of severe infection". Tragically, young children are the most vulnerable, accounting for almost 80 % of all malaria-associated deaths. In 2015, the World Health Organization issued a global technical strategy to address growing concerns around malaria treatment. Sadly, targets set to reduce case incidence and death rates globally, particularly in children, remain unmet.

Until 2009, there was no artemisinin-based combination therapy (ACT) specifically developed for paediatric use. In general, paediatric treatment involved administration of crushed tablets, with dose adjustment. Over the past decade, with increasing recognition of the vulnerability of young children to malaria, as well as the emergence of new drug compounds and combinations that offer improved safety and efficacy, child-friendly antimalarial fixed-dose combination (FDC) products have been marketed. Several formulations have been developed for this purpose including once-daily Eurartesim® (a piperaquine tetraphosphate and artenimol combination) and Pyramax® Granules (sachet containing granules of artesunate and pyronaridine combination) (Medicines for Malaria Venture, 2015). However, undoubtedly, Coartem® which is a taste-masked orodispersible tablet formulation co-developed by the Medicines for Malaria Venture and Novartis (2009)

* Corresponding authors.
E-mail address: g.andrews@qub.ac.uk (G.P. Andrews).

https://doi.org/10.1016/j.ijpharm.2024.124676
Received 20 March 2024; Received in revised form 16 August 2024; Accepted 5 September 2024
Available online 8 September 2024

has gained the most attention for its potential to improve dosing accuracy and patient compliance.

Coartem® is a combination product that provides effective antimalarial treatment through the rapid action of artemether (ART) coupled to long-acting lumefantrine (LUM). Despite Coartem® offering improved patient compliance, it is well known that lumefantrine suffers from poor oral bioavailability, owing to the poor solubility and permeability (Wahajuddin et al., 2011). This leads to a requirement to increase dosing or risk treatment failure (Ogutu et al., 2023). In addition, lumefantrine is highly lipophilic and has been shown to exhibit significant food effects, with a 16-fold bioavailability increase when administered with a high-fat meal (Djimdé and Lefèvre, 2009); (Jain et al., 2017). It is therefore recommended that lumefantrine be administered with a high-fat meal, which can be particularly challenging in poverty-stricken areas, where malaria remains intractable. Moreover, the typical symptoms of malaria, which include vomiting and diarrhoea, are also obstacles to optimal efficacy. Where Coartem® Disperse is used (in paediatric patient), the requirement for water to facilitate dispersion of tablets may also introduce additional risk factors such as potential contamination, particularly where clean water is in short supply.

Recent approaches, reported in the literature, to enhance the therapeutic efficacy of Coartem® include the use of nanoparticles (Armstrong et al., 2023), cyclodextrin nano-sponges (Pawar and Shende, 2020), mesoporous silica (Bhattacharyya and Ramachandran, 2022), microneedle arrays (Volpe-Zanutto et al., 2021), nanocrystals (Hassan Shah et al., 2021) and amorphous solid dispersions (ASDs) (Bhujbal et al., 2021; Trasi et al., 2020). Amongst these, ASDs offer a significant opportunity to enhance the dissolution behaviour of poorly water-soluble drugs, bringing substantial opportunity to overcome the sub-optimal clinical performance of compounds that exhibit dissolution-limiting absorption. Over the course of the last ten years, there have been many techniques employed to manufacture amorphous drug platforms, including spray drying, solvent-evaporation, anti-solvent precipitation and hot melt extrusion (HME) (AL-Japairai et al., 2023; Trasi et al., 2020). In the context of formulating and manufacturing a drug product for extended use across sub-Saharan Africa, affordability and availability are two of the most critical factors that impede widespread access to medication (Armstrong et al., 2023; Yenet et al., 2023). In that case, HME presents particular benefits owing to it being continuous in nature, solvent-free, and easily “scalable”. Moreover, as a continuous process, HME offers the pharmaceutical industry a means of addressing process inefficiencies, improving manufacturing agility and thus, is a processing tool that can be used to enhance product quality whilst reducing production costs (Badman et al., 2019).

ASDs are well-known to be susceptible to physical stability issues during storage (Weuts et al., 2003). The high energy state of amorphous materials is prone to relaxation, leading to recrystallisation and ultimately loss of therapeutic benefit (Zhou et al., 2002). Moreover, physical instability of amorphous drug is often a major challenge in sub-Saharan conditions. Numerous attempts have been reported in the literature to probe not only successful formation of ASDs, but also appropriate stabilisation of these high energy systems. Well-reported stabilising strategies include the use of drug-polymer interactions, mathematical modelling to help select systems having superior drug-polymer miscibility and/or solubility (Tian et al., 2013; Li et al., 2016), physical entrapment either using high glass transition temperature (Tg) polymers or via porous silica-based materials.

This work describes the potential of HME as a continuous and agile drug product manufacturing technology to address the solubility challenges of lumefantrine.

This article investigates the impact of drug loading and HME processing conditions on ASD formation and the resistance of manufactured ASDs to recrystallisation under accelerated conditions. To achieve these aims, this study was set out to: (1) produce ASDs consisting of LUM within Soluplus®-based matrices at two drug loadings (30 % w/w and 50 % w/w respectively); (2) investigate the role of HME processing parameters, including barrel temperature profile and extruder scale, upon drug amorphization in ASDs; (3) understand how oversaturated amorphous drug formulations, manufactured by intense processing, impact drug product performance (stability and drug release characteristics).

2. Materials and methodology

2.1. Materials

Lumefantrine (LUM) was sourced from Kemprotec Limited, UK. Soluplus® (SOL), Kolliphor® SLS Fine (SLS) and Kolliphor® PS80 (T80), were provided by BASF Corporation, USA. High-purity solvents and reagents, including acetonitrile (ACN), methanol (METH), acetone, sodium phosphate tribasic dodecahydrate (TSP) and hydrochloric acid (HCl), essential for HPLC mobile phase and dissolution medium preparation, were procured from Fluka Honeywell, UK. Trifluoroacetic acid (TFA) of analytical grade was obtained from VWR International, UK. All chemicals were used as received.

2.2. Methods

2.2.1. Determination of LUM saturation solubility

The solubility of crystalline LUM powders was assessed in 0.1 N HCl at pH 1.2 in the presence of SLS at concentrations of 0.5 %, 1 %, and 2 % w/v. Approximately 5 mg of LUM was added to 15 ml centrifuge tubes containing 10 ml of the respective medium. These tubes were shaken at 37 ± 0.5 °C at 100 rpm in an orbital incubator for 72 h. After incubation, a 1 ml aliquot was extracted and filtered through a 0.45 μm polyethersulfone (PES) syringe filter (Sarstedt, Germany), then diluted at a 1:4 ratio with ACN containing 0.05 % v/v TFA. The drug content was quantified using high-performance liquid chromatography (HPLC), with each measurement performed in triplicate.

2.2.2. Thermal analysis using differential scanning calorimetry (DSC)

The thermal properties of raw materials and extrudates were analysed using a 214 Polyma DSC (NETZSCH, Germany). Accurately weighed samples (5–10 mg) were placed into aluminium pans (NETZSCH, Selb, Germany) and crimped with aluminium lids prior to measurements. Dry nitrogen at a flow rate of 60 mL/min was used as the purge gas. The various DSC methods employed for different samples are detailed in Table 1. Data was analysed using Proteus thermal analysis 8.0 software (NETZSCH, Germany). All experiments were performed in triplicate and data presented as the mean with standard deviation. Melting point (Tm) of materials were determined using the peak temperature of each respective endothermic event. The glass transition (Tg) temperatures were defined as the midpoint of the transition.

2.2.3. Powder X-ray diffraction (PXRD)

The crystalline structure of the raw materials, physical mixtures, and extrudates was investigated using a Mini-Flex II Powder X-ray Diffractometer (Rigaku™, Japan). PXRD was operated at 30 kV and 15 mA with Cu Kα radiation, with analysis spanning an angular range (2θ) from 1.5° to 40°. Samples were meticulously positioned on a glass sample holder featuring a 0.2 mm indentation for top-loading. The PXRD scans were performed in a continuous mode, employing a sampling width of 0.02° and a scanning speed of 2.0° per minute. .

Temperature variable XRD was conducted using Panalytical Aeris benchtop XRPD equipped with an Anton Paar BTS 500 hot stage. Diffractograms of the samples were typically equilibrated at a set temperature for approximately 2 min, and collected using a scan range 5-35° 2θ, a step size 0.011°, and a counting time 59 s. XRPD were sorted and manipulated using HighScore Plus v4.9 software. All samples used for PXRD analysis in this study were pulverised and sieved to a powder size range between 45–90 μm.

Single crystal data was collected from a suitable single crystal of the

Table 1
A summary of the DSC methods used in this study.

Sample type	1st heating		Cooling		2nd heating	
	Rate (°C/min)	Range (°C)	Rate (°C/min)	Range (°C)	Rate (°C/min)	Range (°C)
Raw materials	10	−20 ~ 160	/	/	/	/
Physical mixtures	10	−60 ~ 160	/	/	/	/
Fresh extrudates	10	−20 ~ 160	/	/	/	/
Stored extrudates	10	−20 ~ 160	/	/	/	/
LUM-HCH 1*	10	−20 ~ 130	30	130 ~ −40	10	−40~160
LUM-HCH 2	10	−20 ~ 170	30	170 ~ −40	10	−40~160

*An isotherm at 130 °C was performed for these runs after completion of the 1st heating. The samples were kept in isotherm for a duration of 10 min, prior to being subjected to the cooling procedure.

lumefantrine that was selected using a Leica M205C light microscope and sperated with oil. Single crystal data was collected for LUM as supplied and from acetone crystallised LUM. The X-ray diffraction experiment was carried out on a Stoe Stadivari with monochromated Mo-Kα radiation and a Pilatus 200 k detector. Measurements were collected at 100 K using an Oxford Cryostream cooling device.

2.2.4. Preparation of the hot-melt extruded ASDs

Two different extruders were utilized for extrudate manufacture, a 10 mm, 20:1 co-rotating, fully intermeshing twin-screw extruder (Horizontal 20/1) (Microlab, Rondol Industrie, France), and a 10 mm, 40:1 co-rotating, fully intermeshing vertical twin-screw extruder (Vertical 40/1) (Vertical all in One, Rondol Industrie, France), both of which utilised a 2 mm. Detailed screw configurations for these processes are presented in Table 2. Binary mixtures of LUM and SOL at weight ratios of 3:7 (F1) and 5:5 (F2), respectively, were mixed by hand using a mortar and pestle. Powdered blends of each formulation were subsequently introduced into the extruder at 30 rpm using a twin-screw powder force feeder (Rondol Industrie, France). The extrusion process across all experimental runs was standardized at a screw speed of 90 rpm, subject to various temperature profiles as outlined in Table 3. Upon exiting from the respective extruder die, the produced filaments were air-cooled, pulverised and sieved into various size ranges (dependent upon characterisation technique), and preserved in a vacuumed desiccator over silica gel prior to further analyses.

The nomenclature of formulations, their respective compositions and extrusion conditions are summarised in Table 4. In general, two different drug loadings were investigated and named F1 and F2, respectively. Where the extrudates were produced using, for example, the Horizontal 20/1 extruder employing the first temperature profile as detailed in Table 3, the extrudates was then named as “F1_HTP1”, “H” for horizontal, “TP1” for temperature profile 1”.

2.2.5. High performance liquid chromatography (HPLC)

LUM concentrations were quantified using an Agilent 1260 Infinity Series High Performance Liquid Chromatography system (Agilent Technologies Ltd, UK). Chromatographic separation was achieved on a Kinetex® Reverse Phase C18 column (150 mm × 4.6 mm, 5 μm particle size, USA), maintained at a constant temperature of 40 °C. The mobile phase comprised a 30:70 v/v mixture of an aqueous solution (0.1 % TFA) and ACN, delivered at a flow rate of 0.8 mL/min. Analyte injection volume was set at 10 μL. Detection was conducted using a UV detector set at a wavelength of 336 nm. A linear relationship between the integrated intensity values for the peak at retention time (Rt) of 2.4 min and the concentrations was confirmed over a LUM concentration range of 1.5–250.0 μg/ml ($y = 15.308x + 8.99$), with a limit of quantification (LoQ) of 0.1 μg/mL, and a correlation coefficient (R^2) exceeding 0.99.

Table 2
Screw configurations used for the horizontal and vertical extruder, respectively.

Type of Element	Number of elements on each shaft Horizontal extruder	Number of elements on each shaft Vertical extruder
Forward convey	5	10
60° Kneading	1	2
90° Kneading	1	2
60° Kneading	1	2
Forward convey	3	6
60° Kneading	1	2
90° Kneading	1	2
60° Kneading	1	2
Forward convey	6	12
Total	**20**	**40**

2.2.6. In-vitro drug dissolution

To evaluate the dissolution characteristics of LUM from extruded samples, *in vitro* drug dissolution tests were conducted in 0.1 N HCL, pH 1.2. This analysis utilized a USP Type II apparatus, specifically a Copley DIS 8000 (Copley Scientific, UK), set to a paddle rotation speed of 100 rpm and a temperature of 37.0 ± 0.5 °C. Milled extrudates, within the particle size range of 125–250 μm and equivalent to a therapeutic dose of LUM (120 mg), were placed in each dissolution vessel containing 500 mL of 0.1 N HCl solution (pH 1.2) with SLS (1 % w/v). Aliquots (2 mL) were sampled at predetermined time intervals: 10, 20, 30, 45, 60, 90 and 120 min, respectively. The sample were immediately filtered through a 0.45 μm polyether sulfone (PES) syringe filter, then diluted 1:4 with acetonitrile containing 0.05 % w/v TFA, and analysed for LUM content using the HPLC.

2.2.7. Polarised light microscopy (PLM)

Polarised light microscopy (PLM, Olympus EP50, Tokyo, Japan) was employed to examine phase behaviour of the LUM recrystallisation in aqueous media. Samples were placed between cross-polarized light filters at x20 magnification. All samples were placed upright on glass slides, ensuring adequate exposure to the objective lens.

2.2.8. Accelerated storage study

The extruded matrices from both the horizontal and the vertical extruders were evaluated at a 2-week and 6-month time point. Samples were stored for these periods using the ICH accelerated stability testing condition, involving a stability chamber set to a controlled temperature of 40.0 ± 0.5 °C and a relative humidity of 75.0 ± 0.5 %. The extrudates were analysed using PXRD and DSC analyses, to determine any alteration in the physical state of LUM within the extruded matrices.

2.2.9. Statistical analysis

As appropriate, statistical analyses were conducted using GraphPad Prism 9 (San Diego, CA, USA). One-way analysis of variance (ANOVA) and Tukey-Kramer’s post hoc tests were used to determine the differences between formulations at various time points during *in-vitro* dissolution. The threshold for statistical significance was established at $P \leq 0.05$ for each comparison.

Table 3
The temperature profiles (TP) used in this study. Note that the values presented are the set temperatures input to the machine control panels. Where deviation of the actual temeprature from the set value occurred, all variances were within the acceptable deviation window of 5 °C, for successful operation.

TP Nomenclature	Extruder L/D	Z1 °C	Z2 °C	Z3 °C	Z4 °C	Z5 °C	Z6 °C	Z7 °C	Z8 °C	Die °C
HTP1	Horizontal 20/1	100	120	130	120	/	/	/	/	100
HTP2		100	120	130	120	/	/	/	/	120
HTP3		105	140	170	170	/	/	/	/	150
VTP1	Vertical 40/1	40	100	120	120	130	130	120	120	120
VTP2		40	100	140	170	170	170	170	150	150

Table 4
Nomeclature of the formulations extruded in this study.

Extrudates	LUM	SOL	Extruder	TP
F1_HTP1	3	7	Horizontal 20/1	HTP1
F1_HTP2	3	7		HTP2
F1_HTP3	3	7		HTP3
F1_VTP1	3	7	Vertical 40/1	VTP1
F1_VTP2	3	7		VTP2
F2_HTP1	5	5	Horizontal 20/1	HTP1
F2_HTP2	5	5		HTP2
F2_HTP3	5	5		HTP3
F2_VTP1	5	5	Vertical 40/1	VTP1
F2_VTP2	5	5		VTP2

3. Results and discussion

3.1. Pre-formulation studies

LUM is a lipophilic (Log P 9.19) (Amin et al., 2013), weakly basic (pKa 9.35) drug that is approved for use in antimalarial combination therapy. It is commercially available in artemisinin-based combination therapy (ACT) products containing artemether (AR). It has been extensively reported that the AR-LUM ACT exhibits erratic bioavailability following oral administration, owing to the extremely low aqueous solubility of LUM, and its susceptibility to P-glycoprotein (P-gp) mediated efflux.

LUM's solubility in aqueous media has been reported in the literature to range from 2.6 ng/mL for crystalline LUM in fasted state-simulated intestinal fluid [FaSSIF] (Jain et al., 2017), to 2–3 μg/mL for amorphous LUM in 50 mM pH 6.8 phosphate buffer (Trasi et al., 2020), depending upon the physical state of LUM, as well as the method of detection. In this current study, the saturated solubility of crystalline LUM powder was not detectable in blank media including de-ionised water, 0.1 N HCl (pH 1.2) and phosphate buffer saline (PBS) pH 6.8. To enhance detectability, saturated solubility studies were repeated with the inclusion of sodium lauryl sulfate (SLS), a common surfactant used in compendial dissolution methods, at various concentrations, in 0.1 N HCl. As illustrated in Fig. 1 the addition of SLS resulted in substantial solubility enhancement, giving saturated solubility values of LUM equal to 24.7 ± 1.7, 50.9 ± 3.0, and 87.0 ± 4.1 μg/mL, for SLS concentrations of 0.5 %, 1 % and 2 % w/v, respectively. Addition of SLS at 1 % w/v in HCl was selected as a discriminatory medium for further dissolution studies, to allow sufficient detection sensitivity, whilst also offering capacity to differentiate the dissolution behaviour of the extruded formulations.

Thermal analysis using DSC suggested that the crystalline LUM powders exhibited a melting onset (Tm onset) at 131.1 ± 0.6 °C with a peak temperature (Tm peak) at 135.3 ± 0.1 °C and an enthalpy of melting of 71.4 ± 2.0 J/g (Fig. 2, LUM). Given that LUM remained amorphous, there was no obvious exothermic crystallisation during cooling, and there was a clear glass transition temperature (Tg) at 22.1 ± 0.8 °C (Fig. 2, LUM HCH-2) during reheating suggests that LUM is a good (Class III) glass former (GF) (Alhalaweh et al., 2014). However, when LUM was quench-cooled with nitrogen or following an isothermal period (10 mins at 130 °C) close to the melting temperature, LUM had a slightly different thermal behaviour. A broad Tg event was evident at 21.5 ± 0.7 °C, a recrystallisation upon reheating, followed by a depressed melting peak at 129.1 ± 1.2 °C (relative to 135.3 ± 0.1 °C) (Fig. 2). Whilst an earlier patent does describe a "polymorphic Form I" for Lumefantrine, which exhibits "a characteristic endothermic absorption between 120 °C and 130 °C" (Shantanu et al., 2006), there is a paucity of information within the literature relating to LUM polymorphism. To examine for the presence of a polymorphic form of LUM, the drug was recrystallised from acetone, and characterised using both DSC and single-crystal XRD. Interestingly, the acetone crystallised LUM had similar thermal behaviour to liquid nitrogen quench-cooled, and isothermally treated (10 mins at 130 °C) LUM, exhibiting a depressed melting point at at 131.7 ± 0.2 °C (Fig. 2). Single crystal XRD of Lum as supplied and acetone crystallised drug revealed that the structure of the drug was similar in both cases, and was monoclinic with the P21 space group (Fig. 3). This agrees with the structure previously reported by de Freitas-Marques et al, (2020). Further VT-PXRD data revealed that samples heated to 130 °C, followed by cooling, had the same XRD pattern as the, as supplied LUM (Fig. 4). This confirms that there was no

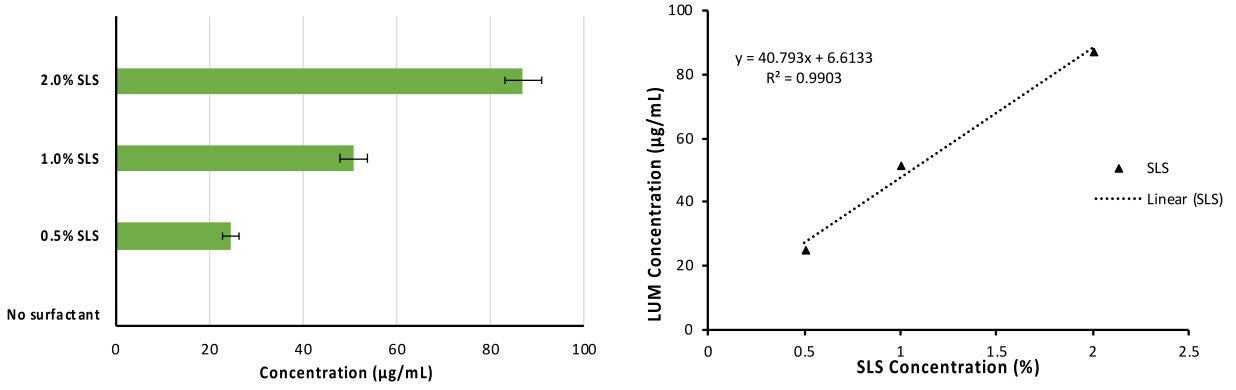

Fig. 1. The impact of surfactant concentration on the saturated solubility of LUM in 0.1 M HCl solution (HCl). Sodium lauryl sulphate (SLS) was added as a surfactant at various concentrations, 0 %, 0.5 %, 1 % and 2 % (w/v), respectively.

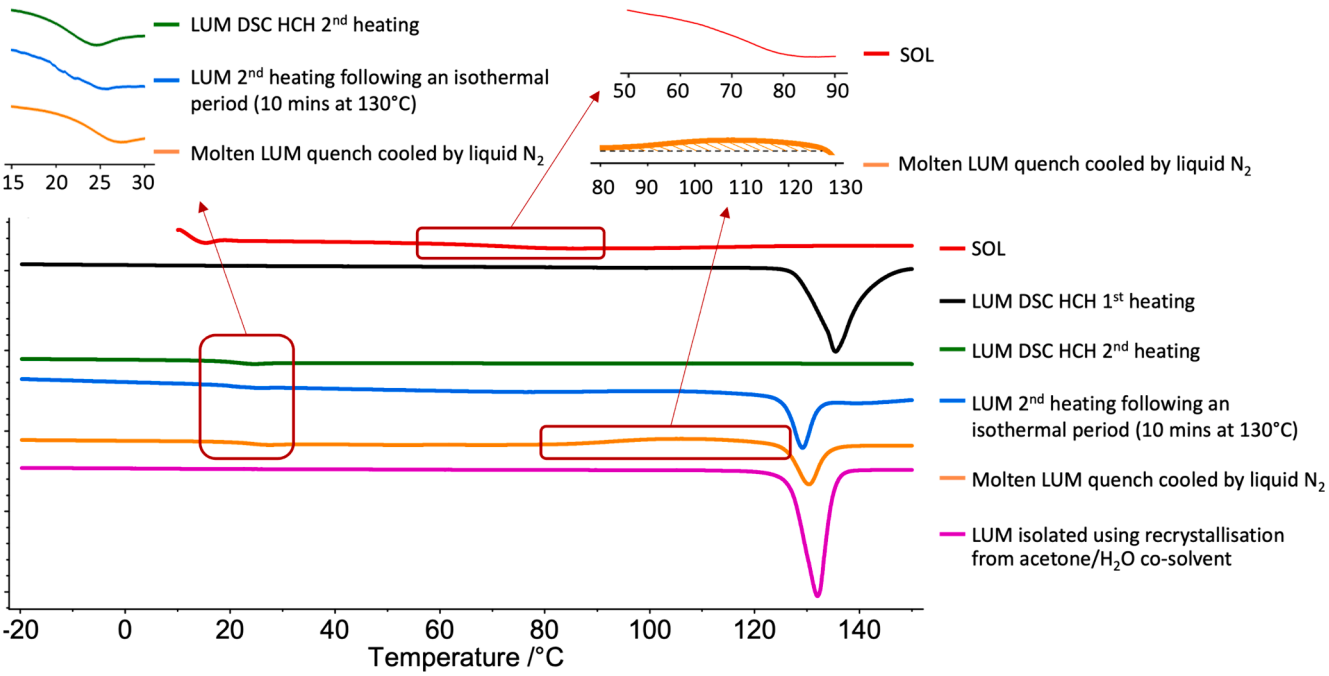

Fig. 2. Representative DSC thermograms of (from top to bottom): Soluplus[@] (SOL); pure LUM on single heating (LUM DSC HCH 1st heating); LUM on second heating of a heat/quench-cool/reheat cycle (LUM DSC HCH 2nd heating); LUM on second heating of a heat/isothermal-quench-cool/reheat cycle (LUM 2[nd]heating following an isothermal period (10 mins at 130 °C)); LUM melted on hot plate followed by quench-cooling using liquid nitrogen (Molten LUM quench cooled by liquid N_2); and LUM recrystallised from an acetone/H2O co-solvent by evaporation (LUM isolated using recrystallisation from acetone/H_2O co-solvent). The Tg regions for SOL amorphous LUM and recrystallisation, respectively, are zoomed-in for improved visibility.

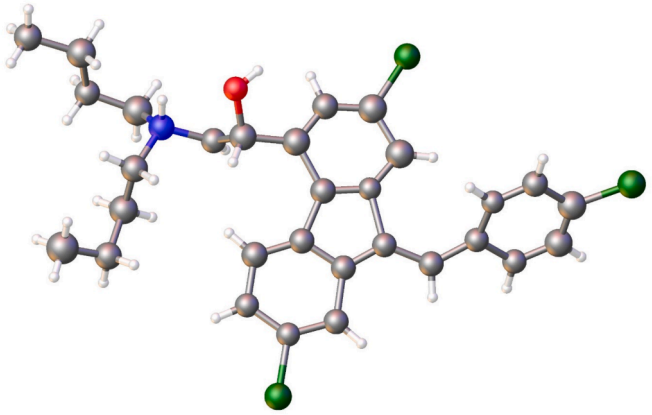

Fig. 3. Crystal structure of LUM as supplied and similar to acetone crystallised LUM (data not shown). Crystal Data for $C_{30}H_{32}NOCl_3$ (M=528.91 g/mol): monoclinic, space group $P2_1$ (no. 4), a = 8.7500(7) Å, b = 9.4127(8) Å, c = 15.7909(10) Å, β = 95.509(7)°, V=1294.55(17) Å^3, Z=2, T=293(2) K, μ(Cu Kα) = 3.386 mm^{-1}, *Dcalc* = 1.357 g/cm^3, 7401 reflections measured (10.156° ≤ 2Θ ≤ 144.37°), 4509 unique (R_{int} = 0.1087, R_{sigma} = 0.1240) which were used in all calculations. The final R_1 was 0.2341 (I>2σ(I)) and wR_2 was 0.6975 (all data).

obvious polymorphic transformation after heating or when crystallised from solvent, albeit powder x-ray diffraction patterns indicated minor peak intensity variations (Fig. 5.).

SOL exhibited a Tg at 76.6 ± 0.8 °C and a characteristic amorphous halo in the PXRD pattern (Fig. 5). Physical mixtures of the LUM-SOL binary blends at 30 % w/w and 50 % w/w LUM loadings were subjected to DSC analysis to better understand LUM solubilisation into SOL. The melting enthalpy of LUM (Fig. 6), was significantly less than expected for the respective weight ratio in the formulation. The decreased melting enthalpy, and loss of crystallinity, may be regarded as dissolution of LUM in SOL, below the Tm of the drug. The observed dissolution is not an equilibrium solubility, since dissolution is kinetically hindered by the viscosity of the molten/rubbery polymer and the time available within the experimental method. However, the information gathered can still be of relevance to HME, owing to the short residence time often observed during extrusion processing. In this work, a 10 °C/min heating ramp would have provided approximately 5 min from the Tg of SOL until the Tm of LUM. The measured crystallinity losses in Table 5 indicate that approximately 10.2 % w/w (out of a max 30 % w/w) of LUM dissolves in F1 whereas approximately 3.5 % w/w (out of a max 50 % w/w) of LUM dissolves in F2. It is worth noting that the resultant LUM apparent solubility in SOL decreases as a function of LUM concentration in the blend. Moreover, a single Tg was evident for both physical mixtures that was significantly lower than the Tg of pure SOL (52.5 °C for the physical mixture of F1 and 48.1 °C for F2). This suggests that LUM was potentially exhibiting a plasticising effect for SOL. The remaining crystalline LUM within the physical blends was detected as a depressed melting temperature because of the presence of polymer (Table 5, Tm column) (Li et al., 2016; Tian et al., 2013).

3.2. Preparation of LUM-SOL ASDs via hot melt extrusion

Extrusion was carried out on F1 and F2 formulations using various processing conditions, including changes to the temperature profile (TP) and the extruder L/D ratio. A summary of the observations made during extrusions is presented in Table 6. During extrusion, it was observed that all F1 formulations were transparent, light-yellow filaments, upon exiting the extrusion die, suggesting high likelihood of solid solution formation. F2 formulations, on the other hand, were opaque when using the 20/1 horizontal extruder at the two lower temperatures (HTP1 and HTP2, respectively). This may be indicative of significant residual crystallinity within the extruded matrices. Increasing the HME temperature to temperatures above the Tm of LUM (F2_HTP3) and scaling to the Vertical 40/1 whilst extruding close to Tm of LUM (F2_VTP1) appeared to considerably reduce the crystalline content, resulting in

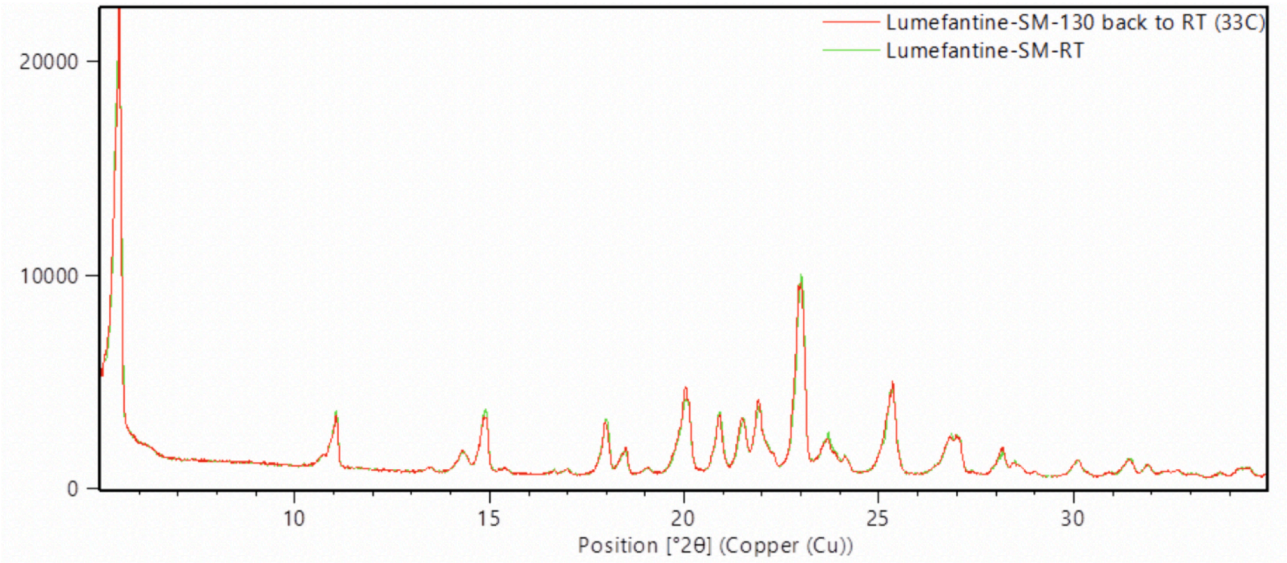

Fig. 4. PXRD patterns of LUM at supplied at room temperature, and heated to 130 °C, cooled and re-run at room temperature.

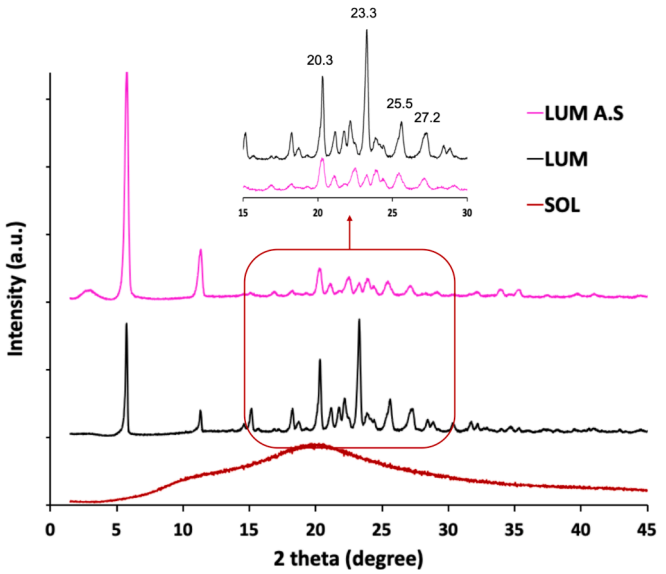

Fig. 5. PXRD patterns of, from top to bottom, LUM recrystallised and isolated from acetone/water (LUM A.S., pink), LUM crystalline powders as supplied (LUM, black) and, SOL powders as supplied (SOL, red), respectively. (For interpretation of the references to colour in this figure legend, the reader is referred to the web version of this article.)

translucent extrudates. Processing using a vertical 40/1 extruder, at temperatures above LUM's Tm (F2_VTP2) resulted in transparent filaments, suggesting a synergistic effect of scaling, vertical processing and temperature elevation, and hence greater levels of amorphization.

The average residence time (Rt) of these formulations within the HME barrel varied dependent upon the type of extruder used. For those formulations extruded using a horizontal 20/1 system, Rt was generally less than 5 min, whereas for the 40/1 vertical system, Rt values were considerably longer (approximately 8 to 10 mins). Such variations in Rt between the two extruders was expected as the extended barrel length increases residence time, especially when screw speed and feeding rate were kept constant. Moreover, with isometrically scaled processing, the number of kneading elements increased. The forward melt flow (transport) efficiency was therefore reduced with the addition of kneading elements, leading to prolonged material residence time. The torque

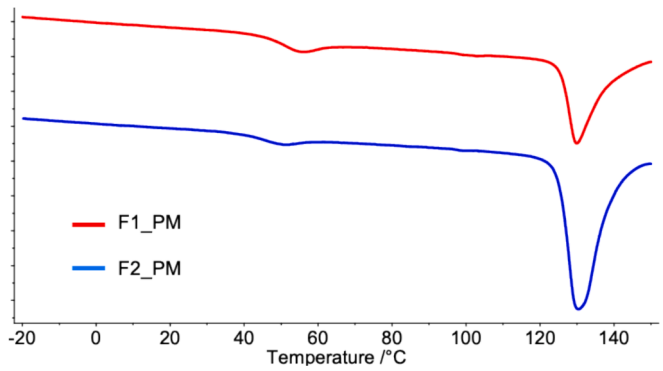

Fig. 6. DSC thermograms of the physical mixtures of F1 and F2 formulations, respectively, on a single heat run from −60 °C using a heating rate of 10 °C/min.

Table 5
Thermal events measured from the F1 and F2 physical mixtures, respectively, on single heating from −60 °C using a heating rate of 10 °C/min. The reported data are mean values and standard deviation from at least three replicates for each mixture.

Test Sample	Tg °C	Tm (onset) °C	Tm (peak) °C	Enthalpy Tm J/g	% LUM crystallinity Lost to "dissolution" of LUM in SOL during heating
F1_PM (30 wt % LUM)	52.5 ± 0.3	126.1 ± 0.0	129.9 ± 0.0	14.1 ± 0.6	34.1 % *
F2_PM (50 wt % LUM)	48.1 ± 0.2	125.7 ± 0.2	130.0 ± 0.4	33.2 ± 1.1	7.0 % *

* Note the % LUM crystallinity loss owing to "dissolution" of LUM in SOL presents the loss as a percentage of the loaded drug content in the respective physical blend.

values observed during extrusion trials followed the above general trend (Table 6), with torque decreasing as temperature increased (comparison of TP1, TP2 and TP3 for both Horizontal and Vertical). Conversely, torque increased, as extrusion scaled from Horizontal to Vertical, for

Table 6
Extrusion parameters recorded during HME processing.

Formulation	Visual Observation	Residence Time (min)	Torque N/m
F1_HTP1	Clear filaments	< 5 min	2.3
F1_HTP2	Clear filaments	< 5 min	1.6
F1_HTP3	Clear filaments	< 5 min	1.2
F1_VTP1	Clear filaments	Approx. 8–10 min	5.0
F1_VTP2	Clear filaments	Approx. 8–10 min	3.2
F2_HTP1	Opaque filaments with dull surface	< 5 min	1.5
F2_HTP2	Opaque filaments with shiny surface	< 5 min	1.5
F2_HTP3	Translucent filaments	< 5 min	0.7
F2_VTP1	Translucent filaments	Approx. 8–10 min	3.2
F2_VTP2	Clear filaments	Approx. 8–10 min	2.9

both F1 and F2. The torque values represent the amount of energy required to rotate the screws and provides important insight into HME processing (Alshetaili et al., 2020). The barrel temperature and the screw speed are usually considered the two most influential factors on torque. In general, elevating HME processing temperature should result in reduced torque values due to softening of material. The screw speed impacts torque by exerting increasing the intensity of shearing, reducing material residence time, and the degree of fill inside the barrel, although the latter two are also influenced by feed rate (Karunanithy and Muthukumarappan, 2011). Torque values typically decrease with increasing screw speed, when feed rate is held constant. This is a result of a decrease in the length of filled screw flights, and an increase in the shear rate (Su et al., 2009) which reduces the resistance on the screws (Meng et al., 2010). In this work, through the use of an isometrically scaled screw configuration, the degree of fill was increased, particularly in the profile where the number of kneading elements increased. This would reduce forward flow of material, and therefore result in an increased torque.

3.3. Understanding drug loading capacity via solid-state characterisation

Extruded formulations were subjected to a solid-state characterisation to gain an understanding of the physical state of LUM within each matrix. As predicted, based on the transparent nature of extruded formulation, the F1 formulations did not contain a characteristic LUM melting endotherm and the formation of a miscible system was further supported by the presence of a single Tg, at a temperature between the Tg values of the polymer and the drug (Fig. 7A). This suggested complete amorphous conversion of the drug within the SOL matrix at 30 % w/w drug loading. A similar conclusion could also be drawn from the PXRD patterns of the F1 formulations, except for F1-HTP1, which was extruded on the 20:1 horizontal extruder with a reduced-temperature TP and the die temperature set to 100 °C. For these processing conditions, we observed two extremely subtle peaks at approximately 5.8° and 23.3° 2θ, characteristic of crystalline LUM (Fig. 8A).

These results were not surprising in that as processing temperature decreased to temperatures below the Tm of the drug substance, drug amorphization becomes driven by the ability of the solid drug particles to "dissolve" within the "molten" (softened) polymeric matrix, rather than "melting" of the drug and mixing with the polymer. Whilst TP1 process settings resulted in small traces of remaining LUM crystallinity following extrusion, at a 30 % w/w drug loading, the quantity of crystalline content was minimal (F1_HTP1). A comparison between F1_HTP1 and F1_PM suggests that extrusion processing led to an enhanced LUM "dissolution" in SOL, increasing the percentage of LUM "dissolved" in

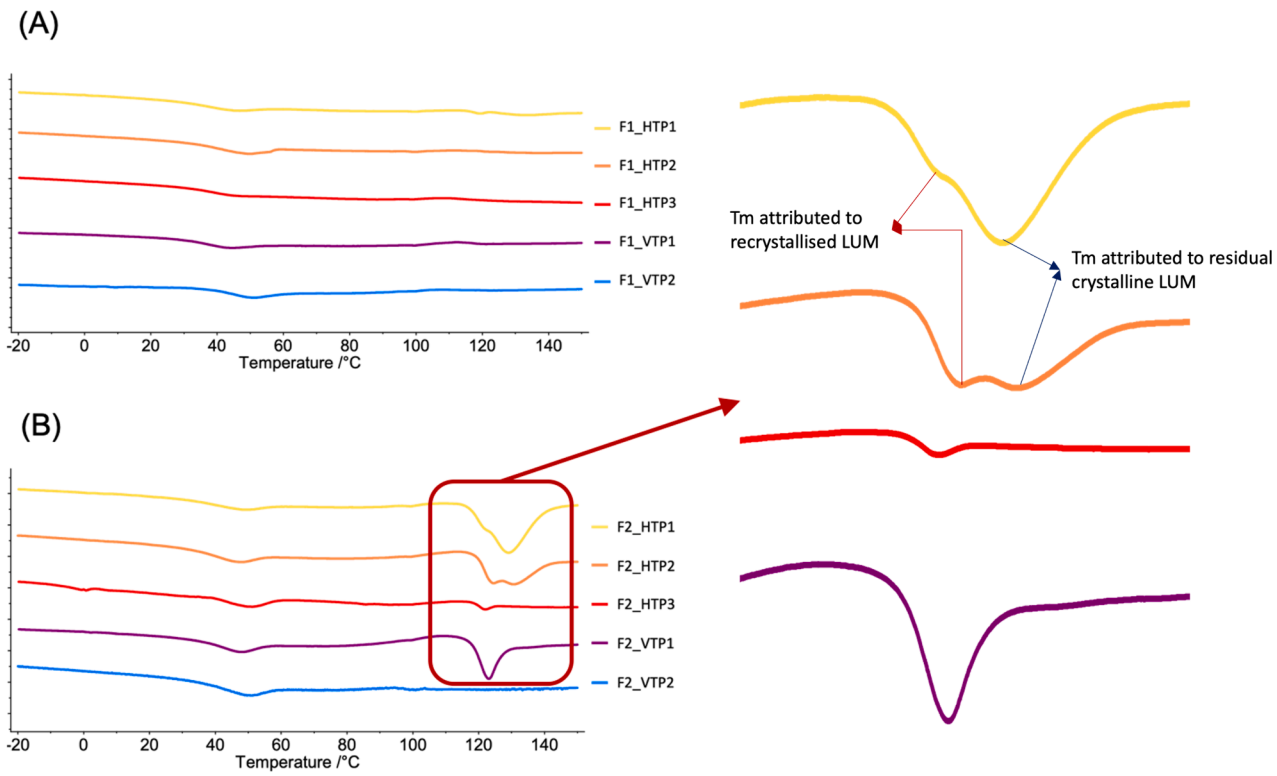

Fig. 7. Representative DSC thermograms of extruded formulations. (A) F1 extrudates and (B) F2 extrudates, processed using, from top to bottom, horizontal extruder with HTP1 (yellow), HTP2 (orange) and HTP3 (red), and vertical extruder with VTP1 (purple) and VTP2 (blue), respectively. The zoomed region illustrates the occurrence of overlapped multiple melting events in the F2_HTP1 and F2_HTP2 extrudates. (For interpretation of the references to colour in this figure legend, the reader is referred to the web version of this article.)

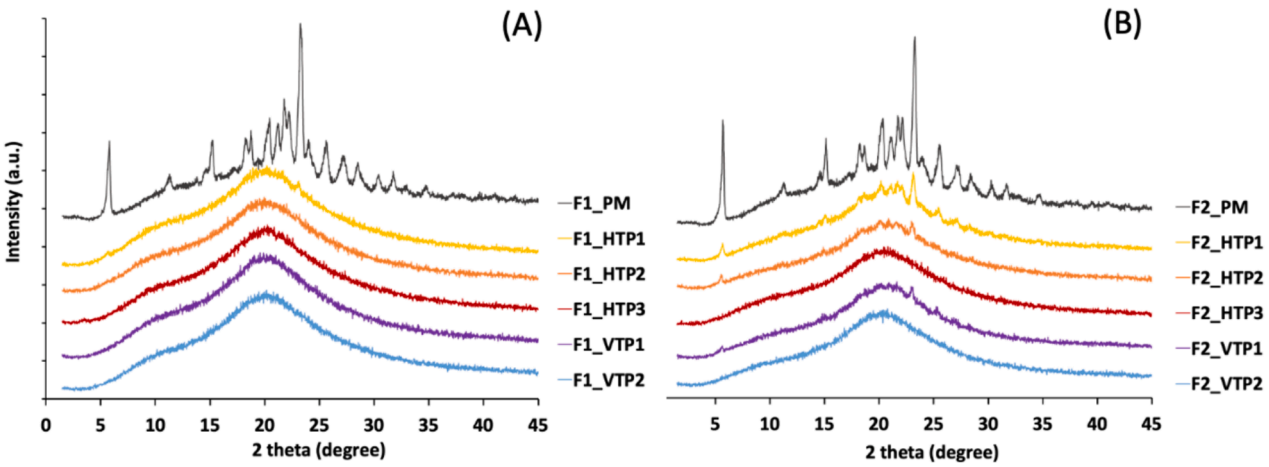

Fig. 8. Representative PXRD patterns of formulations immediately following extrusion. Note that the PXRD pattern of the physical mixture of each formulation is presented at the top of each diffractogram for comparison.

the LUM-SOL binary system from 10.2 % to almost the entirety of 30 % in F1. The formation of these "supersaturated" LUM-in-SOL solutions, particularly for the case of TP1 where zone temperatures were mostly below the Tm of LUM, may be driven by shear forces during HME processing, which act to enhance drug dissolution in the Sol matrix. Upon exiting the extruder, the extrudates readily solidified upon air-cooling thus generating a kinetic barrier to recrystallisation through entrapment of the supersaturated LUM within a glassy Sol matrix.

Formulations (F2 extrudates) containing a higher drug loading (50 % w/w) were somewhat more complex, containing a range of responses that differed according to extruder type and temperature. For F2_HTP1 and F2_HTP2, which were produced using the 20:1 horizontal extruder with zone temperatures mostly set below the Tm of LUM, a Tg was detected followed by a two-step melting (Fig. 7B). In particular, F2_HTP1 exhibited a Tg at 44.4 ± 0.3 °C, and a minor exothermic event just after 100 °C (enthalpy of 1.09 ± 0.1 J/g), a shoulder Tm at 122.0 ± 0.6 °C and a second Tm peak at 129.4 ± 0.2 °C. Formulation F2_HTP2 exhibited a Tg at 46.0 ± 0.5 °C, a small exotherm just after 100 °C (7.9 ± 0.5 J/g), a Tm at 122.5 ± 0.4 °C and a second Tm at 130.8 ± 0.0 °C. The increased residual crystallinity following extrusion of the higher drug loaded formulation F2 was likely the result of having a significant amount of excessive LUM in the formulation melt. At this higher drug loading, which is significantly higher than the saturation solubility, and with a reasonably low processing temperature, these two extrusion profiles are likely to result in a reduced "apparent solubility", due to a higher number of crystallisation surfaces, as well as the lack of time to reach equilibrium.

F2_HTP3, which was produced with zone temperatures set above the Tm of LUM, resulted in a Tg at 40.1 ± 2.7 °C, a very subtle exotherm starting from approximately 105 °C, and a single melting at 122.3 ± 0.2 °C. It was difficult, at the scale of these thermal events, to quantify the heat dissipated during the exotherm or that absorbed during melting. After scaling to a 40/1 vertical extruder, the F2_VTP1 formulation exhibited a Tg at 35.1 ± 1.4 °C, a noticeable exotherm shortly after 100 °C suggesting crystallisation (enthalpy of crystallisation = 7.2 ± 0.6 J/g), and a single Tm at 123.4 ± 0.0 °C (enthalpy of melting = 8.8 ± 0.4 J/g). It is important to note that the enthalpy value of the exothermic crystallisation was almost equivalent to the subsequent melting endotherm, suggesting that the majority of detected crystalline content in the F2_VTP1 extrudates may have resulted from recrystallisation upon heating during DSC analyses. A further increase in the zone temperatures resulted in complete amorphization of LUM in the F2_VTP2 extrudates and no visible evidence of LUM recrystallisation or residual crystallinity during heating within the DSC.

From this data, it can be concluded that this lower Tm event in the region of 122–123 °C may be attributed to recrystallisation of LUM from a supersaturated LUM-SOL "solution". The reduction of Tm, compared to the as supplied LUM, may be due to the formation of a crystal defects, and lowered drug melting. The higher-melting event in both F1_HTP1 and F1_HTP2, on the other hand, is characteristic of the Tm of the as supplied LUM when in presence of SOL. Increasing the HME temperatures (when using TP3) and isometric scaling to a vertical 40/1 extruder were both proven to be effective to reduce the residual crystallinity of F2, resulting in loss of the melting endotherm in DSC. However, where these supersaturated "solutions" were generated by shearing force, they seemed unstable and resulted in LUM recrystallisation upon exposure to external stimuli, such as heating during DSC analysis.

PXRD patterns of the F2 extrudates suggested residual LUM crystallinity in F2_HTP1, F2_HTP2 and F2_VTP1, and a lack of characteristic crystalline diffraction peaks in F2_HTP3 and F2_VTP2 (Fig. 8B). Although PXRD was not used as a quantitative measurement in this study, the intensities of the detected LUM characteristic peaks at 5.8° and 23.3° 2θ, respectively, were noticeably decreased with increasing HME temperature as well as with scaling from a horizontal to vertical extrusion system.

3.4. Stability of the ASDs

The extruded formulations were stored under ICH accelerated conditions for a period of six months, with stored samples being assessed for changes in LUM crystallinity using PXRD and DSC, as well as for drug dissolution performance. In brief, the PXRD patterns of the stored samples suggest that all investigated formulations recrystallised, but to varying extents. (Fig. 9). After 2 weeks most formulations displayed peaks characteristic of crystalline LUM, and an increased drug loading resulted in significant levels of recrystallisation. However, for formulations containing 30 % w/w LUM, F1 VTP1, F1VTP2 and F1HTP3 had a small peak at 5.8° 2θ after 2-weeks storage. After six months of storage, formulations F1 VTP1, F1VTP2 and F1HTP3 had peaks that were more intense but nonetheless they were not as intense as a physical mixture of drug and polymer. This suggested a small increase in drug crystallinity, but not significant enough to suggest complete recrystallisation.

The DSC analyses provided further insights into the recrystallisation of LUM formulations during storage. As illustrated in Fig. 10, after 2-weeks of storage, formulations exhibited a second Tg. This new Tg was present at a temperature lower than that of the binary Tg, suggesting amorphous-amorphous phase separation (AAPS) between LUM and SOL, and formation of LUM-rich amorphous region. There was also evidence of small melting peaks ($\Delta H < 3.5$ J/g) detected in the temperature range 121.0 – 123.0 °C across all stored F1 extrudates, suggesting

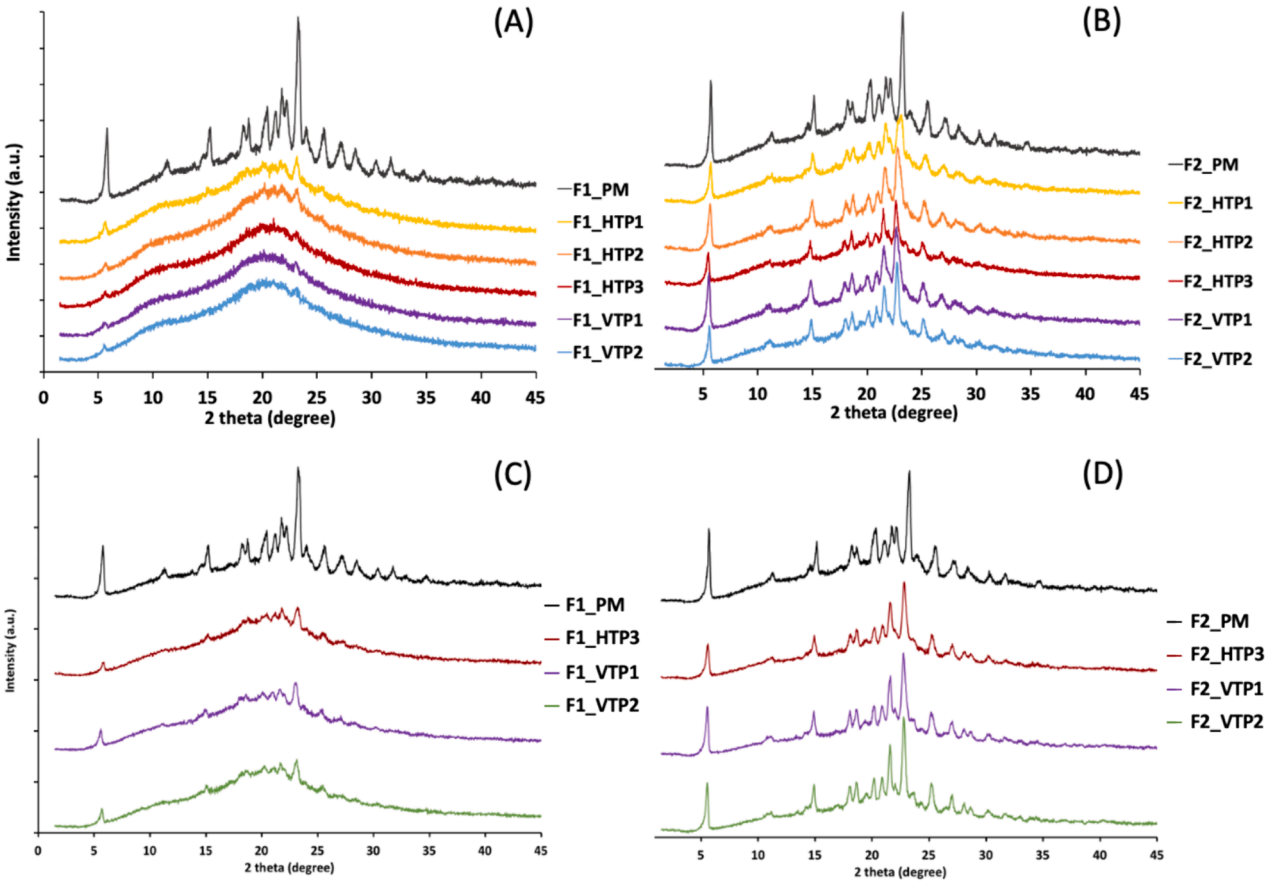

Fig. 9. PXRD patterns of extruded formulations following storage under accelerated conditions (A) F1 extrudates over a 2-week period; (B) F2 extrudates over a 2-week period; (C) F1 extrudates over a 6-month period; and (D) F2 extrudates over a 6-month period. Note that the PXRD pattern of the physical mixture of each formulation is presented at the top of each diffractogram for comparison.

recrystallisation of the loaded LUM content. When HME was conducted above the Tm of LUM (TP3) and/or using the Vertical 40/1, the extruded F1s exhibited a lower melt enthalpy, suggesting lower levels of crystallinity. Similar observations of LUM-SOL amorphous phase separation were observed for F2 formulations, with a more pronounced extent of crystallinity in the aged extrudates, after 2 weeks storage under accelerated storage conditions. Though, it is important to note that there was residual crystalline LUM content in freshly extruded F2_HTP1, F2_HTP2 and F2_VTP1 formulations. Recrystallisation of LUM during storage was not surprising, since amorphous LUM at drug loadings of 30 and 50 % w/w, were judged to be supersaturated within the SOL matrix.

3.5. *In-vitro drug dissolution*

3.5.1. *Dissolution test using 240 μg/mL target dosing*

The drug dissolution behaviour of LUM from the extruded F1 and F2 formulations were compared to that of the crystalline LUM (as supplied), the respective physical mixture of each formulation, and the commercial Riamet® (20 mg/120 mg) tablets. From Fig. 11, it can be seen that the comparison references showed sub-optimal drug dissolution behaviour with the 'as supplied' LUM and the F2 physical mixture showing similar percentage drug release at the 2-hour time point, reaching approximately 16.9 ± 0.2 % and 18.0 ± 0.5 % of total drug content, respectively. The F1 physical mixture, on the other hand, exhibited consistently higher percentage drug release, when compared to the as supplied LUM, throughout testing, resulting in 22.1 ± 0.9 % release at the 2-hour point.

The critical micelle concentration (CMC) for SOL has been reported to be 0.1 % w/w (equivalent to 1 μg/mL) at 37 °C. The concentration of SOL was 240 μg/mL and 336 μg/mL, respectively, for F1 and F2 PMs, far exceeding the CMC. Therefore, the enhanced dissolution of LUM from the lower drug loading F1 PM might be the result of a more pronounced "surfactant-effect" with higher SOL concentration. Nevertheless, neither PM was capable of producing the required solubilisation of LUM. The commercial Riamet® tablets displayed a similar dissolution profile as the crystalline LUM up to 45 min, and thereafter, showed enhanced dissolution behaviour. The final samples taken at the 2-hour point achieved 29.9 ± 1.2 % LUM release from the commercial tablets, approximately 2-fold of that of the pure crystalline LUM. The enhanced performance of the commercially available Riamet® may have been driven by the presence of Tween 80, a surfactant, within the Riamet® formulation.

The three F1 formulations produced using the horizontal 20/1 extruder all exhibited rapid LUM dissolution in the chosen dissolution media, far exceeding Pharmacopeial acceptance criteria for an immediate release oral dosage formulation (Fig. 11A). The three drug dissolution profiles also reached maximum concentration and highest percentage drug release after approximately 30 min. At the end of the 2-hour dissolution study, all three F1_HTP formulations resulted in higher release percentage (84.8 ± 2.3 %, 61.1 ± 3.4 %, and 42.0 ± 1.7 % respectively for F1_HTP1, 2 and 3), than the as supplied crystalline LUM, the F1 physical mixture, and the Riamet® tablets. Similar dissolution behaviours were observed for F1 extrudates produced using isometrically scaled vertical extrusion profile (Fig. 11B), with an initial rapid burst release of drug, forming a supersaturated concentration, followed by recrystallisation and loss of drug in solution.

Increasing HME temperatures by employing VTP2 resulted in enhanced dissolution performance, with formulations reaching

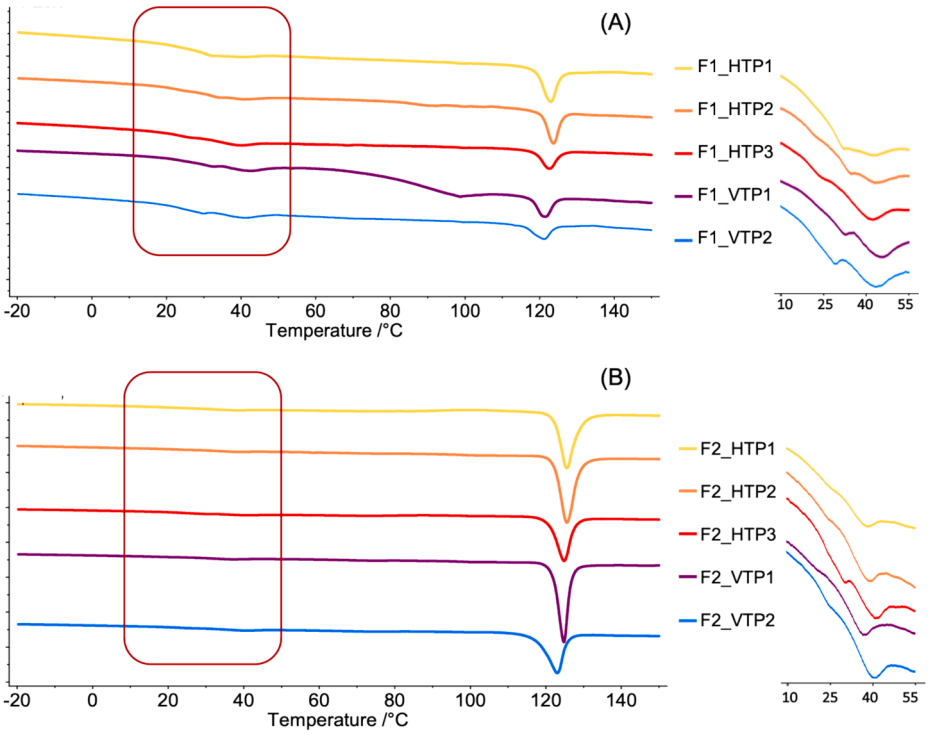

Fig. 10. DSC thermograms of formulations stored for 2 weeks: (A) F1 extrudates and (B) F2 extrudates, processed using, from top to bottom, a horizontal extruder with HTP1 (yellow), HTP2 (orange), and HTP3 (red), and a vertical extruder with VTP1 (purple) and VTP2 (blue), respectively. The expanded regions illustrate the occurrence of phase separation evidenced via separation of a second Tg event. (For interpretation of the references to colour in this figure legend, the reader is referred to the web version of this article.)

complete dissolution within the first 30 min and obtaining a final release percentage of 53.0 ± 6.4 %. It is worth noting that although the F1 vertical extrudates exhibited less dissolution enhancement compared to their respective horizontal counterpart, these extruded formulations still outperformed Riamet® tablets in tested media.

F2 formulations, containing higher drug content, did not enhance the dissolution performance of Lumefantrine as significantly as lower loaded drug formulations (F1). Specifically, F2_HTP2 and F2_HTP3 both resulted in dissolution profiles that were similar to pure drug and the physical mixture equivalent, whilst F2_HTP1 exhibited a similar final percentage release to Riamet® (Fig. 11C). Scaling-up to the 40/1 vertical extruder enhanced the drug dissolution behaviours considerably, with both F2_VTP1 and F2_VTP2 offering an increased extent of LUM dissolution relative to Riamet® alongside a more rapid onset of release (Fig. 11D). The presence of residual crystalline LUM and the instability of amorphized LUM might be a driver for the poor dissolution behaviour of the higher drug loaded F2 formulations. With a high residual crystalline LUM concentration, there is the potential for the drug particles to act as seeding points, with a potential for large number of very small crystalline drug particles (due to high shearing and dispersive mixing to some extent in a TSE) immediately after HME processing. This creates a high tendency for crystallisation and coupled to high LUM supersaturation and lower SOL concentration, recrystallisation may occur rapidly.

The rapid onset and significantly increased drug release of the F1 extrudates were promising. However, the recrystallisation of LUM from solution, as evidenced by rapid decline in drug concentration as a function of time was indicative of physical instability in solution. Recrystallisation kinetics can be complicated, with nucleation and crystal growth from supersaturated solutions being multi-faceted, include factors such as extent of supersaturation, adsorption layer characteristics at the crystal-solution interface and variation in local hydrodynamics. Once recrystallisation occurs during dissolution it is difficult to precisely predict the rate of crystal growth. Moreover, in the investigated ASDs, there was no evidence of intermolecular interaction between LUM and SOL species.

3.5.2. *Dissolution test using 120 μg/mL target dosing*

Initial dissolution testing was conducted run using a LUM dosing equivalent to 240 μg/mL, close to 5-fold the LUM saturation solubility. This dissolution condition was proven to show an excellent discriminatory capacity for the investigated formulations. However, such high supersaturation concentration can bring additional challenges to achieve a satisfactory dissolution profile. To remove these additional challenges, the most promising two candidate F1 formulations were subjected to dissolution, with LUM dosing equivalent to 120 μg/mL. Results of the fresh extrudates shown in Fig. 12, with both formulations conforming to the acceptance criteria for an immediate release formulation in the pharmacopeia alongside steady maintenance of the LUM concentrations towards the end of the 2-hour experiments. The 30 % w/w LUM loaded formulation produced using Vertical 40/1, F1_VTP2, in particular, achieved greater than 4-fold LUM percentage release (92.8 ± 4.5 %), compared to Riamet[@] (21.2 ± 0.9 %), at the 2-hour time point. It is worth noting that the dissolution behaviour of the Riamet[@] tablets were slightly different when the study was conducted in 1 L media, showing a slower rate of release, and reaching a lower final LUM concentration after 2 h. This was potentially caused by the presence of Tween 80, as a surfactant and solubility enhancer, in the Riamet[@] formulation. As the volume of the dissolution media increased, the effective concentration of Tween 80 in the media decreased, hence exhibiting reduced ability to facilitate LUM dissolution.

3.5.3. *Dissolution test using aged formulations at 120 μg/mL target dosing*

Following 6-month aging under accelerated storage conditions, F1_HTP3 and F1_VTP2, subjected to dissolution study again to establish the impact of aging and LUM crystallisation upon drug dissolution. As shown in Fig. 12 aging and loss of LUM amorphous content resulted in decreased dissolution performance for both formulations. F1_HTP3 reached a final percentage drug release at 71.8 ± 0.4 %, whilst F1_VTP2

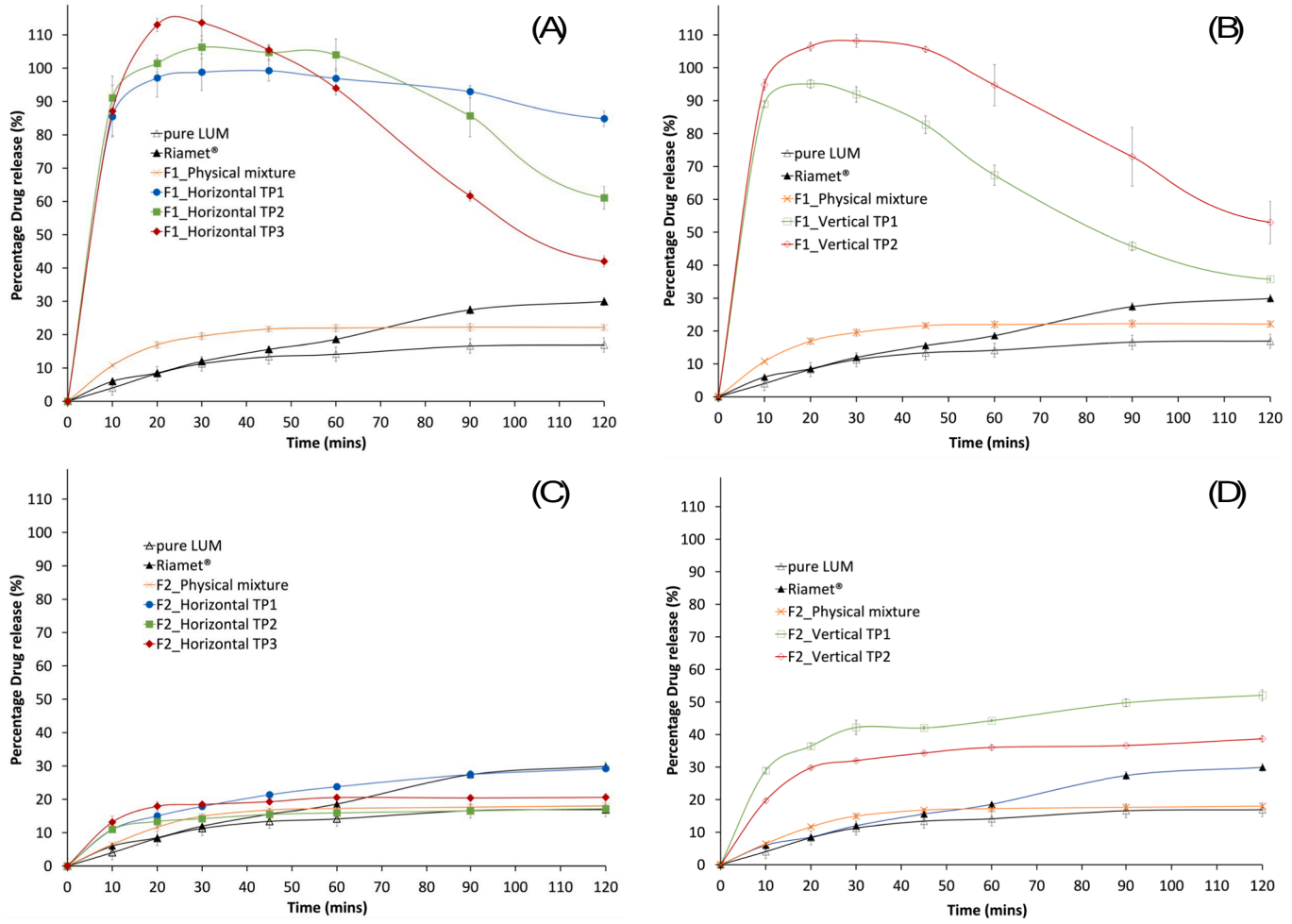

Fig. 11. In-vitro drug dissolution profiles of F1 (30 wt% LUM) and F2 (50 wt% LUM) formulations, extruded using a horizontal and vertical extruder and, using various temperature profiles. Note that these dissolution tests were performed by placing formulations containing equivalent to 120 mg of LUM into 500 mL of 0.1 N HCl solution containing 1 % (w/v) SLS. The dissolution profiles of the as supplied crystalline LUM, the respective physical mixture of each formulation, and the commercial product (Riamet[@]), obtained using the same dissolution method, are plotted as comparison references.

reached 78.4 ± 1.4 %. Although showing considerable reduction, the two aged formulations still outperformed the Riamet[@] tablets by close to 3.5-fold.

4. Conclusion

In this work, hot-melt extrusion was used to probe the drug loading capacity of Soluplus® to accommodate lumefantrine in a binary amorphous solid dispersion. This was used as an example of challenging drug compounds that possess extremely low aqueous solubility and strong tendency for self-aggregation. It was found that via adjustment of extrusion conditions, dissolution performance of F1 solutions (30 % drug loading), even after 6 months aging, outperformed the Riamet tablets by approximately 3.5-fold. The high supersaturation concentration of LUM in these ASDs, however, renders the extrudates susceptible to recrystallisation when exposed to high temperature and or humidity.

The results presented in this work provide evidence for the need to balance high drug loading in an amorphous solid dispersion with physical stability and drug release enhancement. It is possible to achieve high amorphous drug loadings using techniques such as HME are utilised, however formulation success is highly dependent formulation factors, i.e. presence of drug polymer interactions, sufficient physical hindrance to prevent rapid recrystallisation. This is an important note when generating an ideal design space for ASD formulations and should be used to balance processing and formulation design spaces to success.

CRediT authorship contribution statement

Shu Li: Writing – review & editing, Writing – original draft, Supervision, Methodology, Conceptualization. **Zi'an Zhang:** Data curation, Investigation. **Wenjie Gu:** Investigation. **Maël Gallas:** Writing – review & editing, Supervision, Project administration, Conceptualization. **David Jones:** Writing – review & editing. **Pascal Boulet:** Methodology, Investigation, Data curation. **Lindsay M. Johnson:** Writing – original draft, Supervision, Project administration, Conceptualization. **Victoire de Margerie:** Writing – review & editing, Writing – original draft, Supervision, Conceptualization. **Gavin P Andrews:** Writing – review & editing, Writing – original draft, Supervision, Conceptualization.

Declaration of competing interest

The authors declare the following financial interests/personal relationships which may be considered as potential competing interests: [Lindsay M Johnson reports a relationship with BASF Corp that includes: employment. Victoire de Margerie reports a relationship with Rondol Industrie that includes: employment. Maël Gallas reports a relationship with Rondol Industrie that includes: employment. If there are other authors, they declare that they have no known competing financial

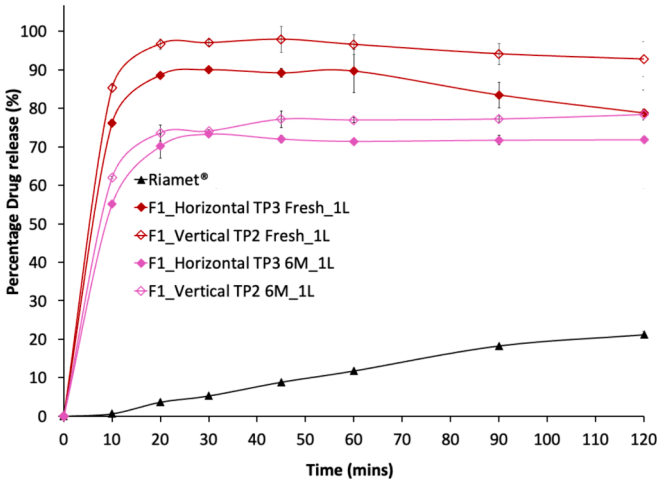

Fig. 12. In-vitro drug dissolution profiles of the two most promising F1 formulations, F1_HTP3 and F1_VTP2, respectively, following storage under accelerated conditions for 6 months. Note that these dissolution tests were performed by putting formulations containing equivalent to 120 mg of LUM into 1 L of 0.1 N HCl solution containing 1 % (w/v) SLS. The dissolution profile of the commercial product (Riamet@), obtained using the same dissolution method, is plotted as comparison references. The dashed line represents the measured saturated solubility of crystalline LUM powders in the same medium.

interests or personal relationships that could have appeared to influence the work reported in this paper.].

Data availability

Data will be made available on request.

REFERENCEs

Alhalaweh, A., Alzghoul, A., Kaialy, W., Mahlin, D., Bergström, C.A.S., 2014. Computational predictions of glass-forming ability and crystallization tendency of drug molecules. Mol. Pharm. 11, 3123–3132. https://doi.org/10.1021/mp500303a.

AL-Japairai, K., Hamed Almurisi, S., Mahmood, S., Madheswaran, T., Chatterjee, B., Sri, P., Azra Binti Ahmad Mazlan, N., Al Hagbani, T., Alheibshy, F., 2023. Strategies to improve the stability of amorphous solid dispersions in view of the hot melt extrusion (HME) method. Int. J. Pharm. Doi: 10.1016/j.ijpharm.2023.123536.

Alshetaili, A., Alshahrani, S.M., Almutairy, B.K., Repka, M.A., 2020. Hot Melt Extrusion Processing Parameters Optimization. Processes 8, 1516. https://doi.org/10.3390/pr8111516.

Amin, N.C., Fabre, H., Blanchin, M.D., Montels, J., Aké, M., 2013. Determination of artemether and lumefantrine in anti-malarial fixed-dose combination tablets by microemulsion electrokinetic chromatography with short-end injection procedure. Malar J. 12. https://doi.org/10.1186/1475-2875-12-202.

Armstrong, M., Wang, L., Ristroph, K., Tian, C., Yang, J., Ma, L., Panmai, S., Zhang, D., Nagapudi, K., Prud'homme, R.K., 2023. Formulation and scale-up of fast-dissolving lumefantrine nanoparticles for oral malaria therapy. J. Pharm. Sci. 112, 2267–2275. https://doi.org/10.1016/j.xphs.2023.04.003.

Badman, C., Cooney, C.L., Florence, A., Konstantinov, K., Krumme, M., Mascia, S., Nasr, M., Trout, B.L., 2019. Why we need continuous pharmaceutical manufacturing and how to make it happen. J. Pharm. Sci. 108, 3521–3523. https://doi.org/10.1016/j.xphs.2019.07.016.

Bhattacharyya, S., Ramachandran, D., 2022. Solubility enhancement study of lumefantrine by formulation of liquisolid compact using mesoporous silica as a novel adsorbent. Mater. Lett.: X 16, 100171. https://doi.org/10.1016/j.mlblux.2022.100171.

Bhujbal, S.V., Pathak, V., Zemlyanov, D.Y., Taylor, L.S., Zhou, Q., (Tony), 2021. Physical stability and dissolution of lumefantrine amorphous solid dispersions produced by spray anti-solvent precipitation. J Pharm Sci 110, 2423–2431. https://doi.org/10.1016/j.xphs.2020.12.033.

de Freitas-Marques, M.B., Yoshida, M.I., Fernandes, B.L., Mussel, W.N., 2020. Lumefantrine Comparative Study: single crystal, powder X-ray Diffraction, Hirschfeld Surface and Thermal Analysis. J. Struct. Chem. 61, 151–159.

Djimdé, A., Lefèvre, G., 2009. Understanding the pharmacokinetics of Coartem®. Malar J 8, 1–8. https://doi.org/10.1186/1475-2875-8-S1-S4.

Hassan Shah, S.M., Mukarram Shah, S.M., Khan, S., Ullah, F., Ali Shah, S.W., Ghias, M., Shahid, M., Smyth, H.D., Hussain, Z., Sohail, M., Elhissi, A., Isreb, M., 2021. Efficient design to fabricate smart Lumefantrine nanocrystals using DENA® particle engineering technology: Characterisation, in vitro and in vivo antimalarial evaluation and assessment of acute and sub-acute toxicity. J. Drug Deliv. Sci. Technol. 61, 102228. https://doi.org/10.1016/j.jddst.2020.102228.

Jain, J.P., Leong, F.J., Chen, L., Kalluri, S., Koradia, V., Stein, D.S., Wolf, M.-C., Sunkara, G., Kota, J., 2017. Bioavailability of Lumefantrine Is Significantly Enhanced with a Novel Formulation Approach, an Outcome from a Randomized, Open-Label Pharmacokinetic Study in Healthy Volunteers.

Karunanithy, C., Muthukumarappan, K., 2011. Influence of extruder and feedstock variables on torque requirement during pretreatment of different types of biomass - A response surface analysis. Biosyst. Eng. 109, 37–51. https://doi.org/10.1016/j.biosystemseng.2011.02.001.

Li, S., Tian, Y., Jones, D.S., Andrews, G.P., 2016. Optimising drug solubilisation in amorphous polymer dispersions: rational selection of hot-melt extrusion processing parameters. AAPS PharmSciTech 17, 200–213. https://doi.org/10.1208/s12249-015-0450-6.

Medicines for Malaria Venture, 2015. PRESS RELEASE Pyramax ® Granules becomes first paediatric antimalarial to receive EMA article 58 positive scientific opinion.

Meng, X., Threinen, D., Hansen, M., Driedger, D., 2010. Effects of extrusion conditions on system parameters and physical properties of a chickpea flour-based snack. Food Res. Int. 43, 650–658. https://doi.org/10.1016/j.foodres.2009.07.016.

Ogutu, B., Yeka, A., Kusemererwa, S., Thompson, R., Tinto, H., Toure, A.O., Uthaisin, C., Verma, A., Kibuuka, A., Lingani, M., Lourenço, C., Mombo-Ngoma, G., Nduba, V., N'Guessan, T.L., Nassa, G.J.W., Nyantaro, M., Tina, L.O., Singh, P.K., El Gaaloul, M., Marrast, A.C., Chikoto, H., Csermak, K., Demin, I., Mehta, D., Pathan, R., Risterucci, C., Su, G., Winnips, C., Kaguthi, G., Fofana, B., Grobusch, M.P., 2023. Ganaplacide (KAF156) plus lumefantrine solid dispersion formulation combination for uncomplicated Plasmodium falciparum malaria: an open-label, multicentre, parallel-group, randomised, controlled, phase 2 trial. Lancet Infect. Dis. 23, 1051–1061. https://doi.org/10.1016/S1473-3099(23)00209-8.

Pawar, S., Shende, P., 2020. Dual drug delivery of cyclodextrin cross-linked artemether and lumefantrine nanosponges for synergistic action using 23 full factorial designs. Colloids Surf. A Physicochem. Eng. Asp. 602, 125049. https://doi.org/10.1016/j.colsurfa.2020.125049.

Shantanu, D., Mohammad, R., Swargam, S.-N., 2006. Polymorphic form I of lumefantrine and processes for its preparation. PCT/IB2006/001037.

Su, B., Xie, F., Li, M., Corrigan, P.A., Yu, L., Li, X., Chen, L., 2009. Extrusion processing of starch film. Int. J. Food Eng. 5. https://doi.org/10.2202/1556-3758.1617.

Tian, Y., Booth, J., Meehan, E., Jones, D.S., Li, S., Andrews, G.P., 2013. Construction of drug-polymer thermodynamic phase diagrams using flory-huggins interaction theory: Identifying the relevance of temperature and drug weight fraction to phase separation within solid dispersions. Mol. Pharm. 10, 236–248. https://doi.org/10.1021/mp300386v.

Trasi, N.S., Bhujbal, S.V., Zemlyanov, D.Y., Zhou, Q., (Tony), Taylor, L.S., 2020. Physical stability and release properties of lumefantrine amorphous solid dispersion granules prepared by a simple solvent evaporation approach. Int J Pharm X 2, 100052. https://doi.org/10.1016/j.ijpx.2020.100052.

Volpe-Zanutto, F., Ferreira, L.T., Permana, A.D., Kirkby, M., Paredes, A.J., Vora, L.K., P. Bonfanti, A., Charlie-Silva, I., Raposo, C., Figueiredo, M.C., Sousa, I.M.O., Brisibe, A., Costa, F.T.M., Donnelly, R.F., Foglio, M.A., 2021. Artemether and lumefantrine dissolving microneedle patches with improved pharmacokinetic performance and antimalarial efficacy in mice infected with Plasmodium yoelii. J. Controlled Release 333, 298–315. Doi: 10.1016/j.jconrel.2021.03.036.

Wahajuddin, Singh, S.P., Raju, K.S.R., Nafis, A., Puri, S.K., Jain, G.K., 2011. Intravenous pharmacokinetics, oral bioavailability, dose proportionality and in situ permeability of anti-malarial lumefantrine in rats. Malar J 10, 1–9. Doi: 10.1186/1475-2875-10-293.

Weuts, I., Kempen, D., Six, K., Peeters, J., Verreck, G., Brewster, M., Van Den Mooter, G., 2003. Evaluation of different calorimetric methods to determine the glass transition temperature and molecular mobility below Tg for amorphous drugs. Int. J. Pharm. 259, 17–25. https://doi.org/10.1016/S0378-5173(03)00233-3.

World Health Organization, 2022. World Malaria Report 2022.

Yenet, A., Nibret, G., Tegegne, B.A., 2023. Challenges to the availability and affordability of essential medicines in african countries: a scoping review. ClinicoEconom. Outcomes Res. https://doi.org/10.2147/CEOR.S413546.

Zhou, D., Zhang, G.G.Z., Law, D., Grant, D.J.W., Schmitt, E.A., 2002. Physical stability of amorphous pharmaceuticals: Importance of configurational thermodynamic quantities and molecular mobility. J. Pharm. Sci. 91, 1863–1872. https://doi.org/10.1002/jps.10169.